


RESEARCH ARTICLE

WILEY

Altered default mode network causal connectivity patterns in autism spectrum disorder revealed by Liang information flow analysis

Jing Cong¹  | Wenwen Zhuang¹ | Yunhong Liu¹ | Shunjie Yin¹ | Hai Jia¹ |
 Chanlin Yi² | Kai Chen¹ | Kaiqing Xue³ | Fali Li² | Dezhong Yao² |
 Peng Xu² | Tao Zhang¹

¹Mental Health Education Center and School of Science, Xihua University, Chengdu, China

²The Clinical Hospital of Chengdu Brain Science Institute, MOE Key Lab for Neuroinformation, University of Electronic Science and Technology of China, Chengdu, China

³School of Computer and Software Engineering, Xihua University, Chengdu, China

Correspondence

Peng Xu, The Clinical Hospital of Chengdu Brain Science Institute, MOE Key Lab for Neuroinformation, University of Electronic Science and Technology of China, Chengdu, China.
 Email: xupeng@uestc.edu.cn

Tao Zhang, Mental Health Education Center and School of Science, Xihua University, Chengdu, China.
 Email: zhangtao1698@mail.xhu.edu.cn

Funding information

National Natural Science Foundation of China, Grant/Award Numbers: #62006197, #61961160705, #U19A2082; The Project of Science and Technology Department of Sichuan Province, Grant/Award Number: #2018JY0526

Abstract

Autism spectrum disorder (ASD) is a pervasive developmental disorder with severe cognitive impairment in social communication and interaction. Previous studies have reported that abnormal functional connectivity patterns within the default mode network (DMN) were associated with social dysfunction in ASD. However, how the altered causal connectivity pattern within the DMN affects the social functioning in ASD remains largely unclear. Here, we introduced the Liang information flow method, widely applied to climate science and quantum mechanics, to uncover the brain causal network patterns in ASD. Compared with the healthy controls (HC), we observed that the interactions among the dorsal medial prefrontal cortex (dMPFC), ventral medial prefrontal cortex (vMPFC), hippocampal formation, and temporo-parietal junction showed more inter-regional causal connectivity differences in ASD. For the topological property analysis, we also found the clustering coefficient of DMN and the In-Out degree of anterior medial prefrontal cortex were significantly decreased in ASD. Furthermore, we found that the causal connectivity from dMPFC to vMPFC was correlated with the clinical symptoms of ASD. These altered causal connectivity patterns indicated that the DMN inter-regions information processing was perturbed in ASD. In particular, we found that the dMPFC acts as a causal source in the DMN in HC, whereas it plays a causal target in ASD. Overall, our findings indicated that the Liang information flow method could serve as an important way to explore the DMN causal connectivity patterns, and it also can provide novel insights into the neuromechanisms underlying DMN dysfunction in ASD.

KEYWORDS

autism spectrum disorder, causal connectivity, default mode network, Liang information flow

This is an open access article under the terms of the [Creative Commons Attribution-NonCommercial-NoDerivs](https://creativecommons.org/licenses/by-nc-nd/4.0/) License, which permits use and distribution in any medium, provided the original work is properly cited, the use is non-commercial and no modifications or adaptations are made.

© 2023 The Authors. *Human Brain Mapping* published by Wiley Periodicals LLC.

1 | INTRODUCTION

Autism spectrum disorder (ASD) is a pervasive neurodevelopmental disorder worldwide, with point prevalence exceeding $\sim 1\%$ (Rolls et al., 2020). Individuals with ASD mainly exhibit severe difficulties in social interaction and communication, as well as restricted and repetitive stereotyped behaviors (American Psychiatric Association, 2013). Yet, the pathophysiology of ASD remains unknown. Most previous studies have reported that the abnormal functional connectivity patterns within and between the default mode network (DMN) are highly related to the clinical symptoms of ASD (Assaf et al., 2010; Feng et al., 2022; Lombardo et al., 2019). However, the causal connectivity pattern within the DMN in ASD, which is believed to provide an important clue to understanding the underlying neuro-mechanism of ASD, remains largely unclear.

The DMN is a large-scale brain network that shows reduced activity when the participants perform a task and becomes more active when they are at rest (Bathelt & Geurts, 2021; Raichle et al., 2001). It consists of a set of brain regions, including posterior cingulate cortex (PCC), medial prefrontal cortex (MPFC), precuneus, and the medial, lateral, and inferior parietal regions (Andrews-Hanna et al., 2010; Chen et al., 2021), responsible for self-reference processing (Broyd et al., 2009; D'Argembeau et al., 2005; Gusnard et al., 2001), autobiographical memory (Nielsen et al., 2014), social cognition (Mars et al., 2012; Schilbach et al., 2008), emotional processing (Broyd et al., 2009), theory of mind (ToM) (Chen et al., 2021; Saxe & Kanwisher, 2003), and so on. Numerous neuroimaging studies have demonstrated abnormal DMN structure and function in ASD (Lynch et al., 2013; Monk et al., 2009; Padmanabhan et al., 2017). For instance, Lynch et al. (2013) found that the over-connectivity of the PCC and precuneus within DMN is related to the social severity of ASD. Padmanabhan et al. (2017) showed that PCC, dorsal and ventral MPFC, and temporal-parietal junction (TPJ) play distinct interacting roles in monitoring the mental state of the self and the evaluation of others. Monk et al. (2009) found that the functional connectivity (FC) between the PCC and superior frontal gyrus was decreased, while the FC between the PCC and the right temporal lobe and right parahippocampal gyrus were increased in ASD by comparing with the control group. In our previous study, we also found that low intra-DMN FC variability was associated with social deficits in ASD (Feng et al., 2022). However, these studies are mainly based on FC analysis, which cannot capture the direction of information interaction.

FC refers to the spatial-temporal correlation between brain regions without the flow of information (Biswal et al., 1995), while effective connectivity (EC) refers to the causal influence exerted by one brain region on another (Kamiński et al., 2001). Recently, many studies have demonstrated that causal connections in brain networks can better reflect the interactions between brain regions (Rolls et al., 2020; Talebi et al., 2019). Compared with FC analysis, EC or causal connectivity analysis can not only evaluate the interaction strength between brain regions, but also capture the flow of information. Several common methods are widely used in constructing causal connectivity networks, such as Granger causality analysis (GCA) and transfer entropy (TE). GCA uses a data-driven method to infer the

causal relationship between multivariate time series based on multivariate autoregressive (MVAR) (Venkatesh & Grover, 2015). Sridharan et al. (2008) found that the right anterior insula plays an important causal role in switching the DMN and executive-control network (ECN) during cognitive information processing using the GCA. Wang et al. (2020) found that the MPFC showed significant causal influences on the PCC within the DMN in healthy subjects using the GCA. Transfer entropy (TE) is an extension of the concept of mutual information, which is based entropy to infer quantified information transfer (Schreiber, 2000). For example, Zhao et al. (2021) found the decreased causal connectivity from right ventral posterior cingulate cortex to right ventral anterior cingulate cortex and increased causal connectivity from right dorsal frontal cortex to left piriform cortex within the DMN in ASD using entropy connectivity. Dejman et al. (2017) also found a significant difference in average degree between HC and ASD groups during a passive face processing task by integrating transfer entropy and graph theory.

Although traditional causal analysis methods provide new perspectives for causal network construction, they have shortcomings in their application. For example, GCA makes assumptions in the calculation process (Harmah et al., 2020), and it requires stationarity of the time series analyzed in the GCA calculation. Furthermore, GCA measures causal relation in a statistical sense, and a larger GCA value does not necessarily mean a higher true causal relation (Harmah et al., 2020). TE requires long time series, and the computation is complex (Hlaváčková-Schindler et al., 2007). Recently, Liang proposed a novel method to calculate the causal relation, namely Liang information flow (Liang, 2008; Liang, 2014; Liang, 2016b; Liang & Kleeman, 2005). Liang (2014) defined the calculation method of Liang information flow through a rigorously derived formalism and gave a specific calculation expression. The Liang information flow method have been shown to be effective in capturing the causal relation between time series (Liang, 2021; Zhang et al., 2021), and has been widely applied to a variety of fields in different disciplines, such as quantum mechanics (Yi & Bose, 2022), climate science (Cheng & Redfern, 2022; Docquier et al., 2022; Liang et al., 2021), brain electroencephalography (EEG) network (Hristopoulos et al., 2019). Its advantages include its very effective performance in computing, as well as its accuracy, and, most of all, its universal applicability because of its firm physical ground, and hence many intrinsic properties that make accurate causal discovery possible. Thus, the Liang information flow method can provide a new effective way to capture the causal connectivity within the DMN.

In this study, we combined the Liang causal information flow method and graph theory to investigate the resting-state DMN causal connectivity patterns in ASD and HC. We first construct the DMN causal connectivity networks for the two groups using the Liang information flow. We then compared the differences in causal network connectivity patterns between the two groups. Finally, we also correlated the causal connectivity patterns to the ASD symptom severity scores to better understand the underlying neural mechanism of ASD. In addition, using the causal connectivity patterns as features, we construct a classification model for identifying ASD. Our results provide a novel perspective for understanding the DMN causal connectivity pattern in ASD.

2 | MATERIALS AND METHOD

2.1 | Participants

The study includes 79 patients with ASD and 105 healthy controls (HCs). All subjects are recruited from the public site at NYU Langone Medical Center in ABIDE (http://fcon_1000.projects.nitrc.org/indi/abide/) (Di Martino et al., 2014). The criteria for the inclusion of the subjects were as follows: (1) age between 6 and 18 years old; (2) head motion not exceeding 2 mm translation or 2° rotation in any direction; (3) subjects with mean framewise displacement (FD) (Power et al., 2012) below mean + 2 × SD; (4) subjects with complete scanned images. Finally, 48 ASD patients (42 boys, six girls; age: 6–18 years) and 48 HC subjects (39 boys, nine girls; age: 6–18 years) were selected for our study. The Autism Diagnostic Observation Schedule (ADOS) (Lord et al., 2000) and Autism Diagnostic Interview-Revised (ADI-R) (Lord et al., 1994) were used as clinical symptoms assessment for further analysis. The detailed demographic information for the included participants is listed in Table 1.

2.2 | Resting-state fMRI data acquisition

All original resting-state images of participants were scanned by 3 Tesla Siemens Allegra scanner using an echo-planar imaging (EPI) sequence with whole-brain coverage. During the resting-state fMRI scan, most participants were instructed to open their eyes and relax while projecting a white crosshair on a screen against a black

background. The acquisition parameters of the resting state fMRI images are: repetition time (TR) = 2000 ms, echo time (TE) = 15 ms, slice number = 33, slice thickness = 4.0 mm, flip angle (FA) = 90°, field of view = 240 mm, voxel size = 3.0 × 3.0 × 4.0 mm³. For each subject, a 6-min scanning was performed, resulting in 180 volumes.

2.3 | fMRI data preprocessing

All original resting-state fMRI data were preprocessed using the Data Processing Assistant for Resting-State fMRI toolbox (Yan & Zang, 2010) (DPARSF, <http://rfmri.org/DPARSF>), which is based on the Statistical Parametric Mapping 12 toolbox (SPM12, <https://www.fil.ion.ucl.ac.uk/spm/>) on the MATLAB 2018a platform. The first 10 volumes were removed to ensure the magnetic field was stable, leaving 170 volumes. All the blood-oxygen-level-dependent (BOLD) time series were corrected for temporal differences in slice timing. Then, head movement correction was performed. All images were normalized to the standard Montreal Neurological Institute (MNI) space, and the voxel size after normalization was 3 × 3 × 3 mm³. All normalized images were smoothed with a Gaussian kernel (full width at half maximum = 6 mm) and then linearly detrended. The signals from the white matter, cerebrospinal fluid, 24 rigid body motion parameters, and head motion scrubbing regressors were regressed from the data. The head motion scrubbing regressors were applied with an FD threshold above 0.5 as well as two back and one forward neighbor. Global signal regression (GSR) is still controversial in resting-state research. Several studies show that using GSR may produce

TABLE 1 The demographics of the participants

	ASD (n = 48)	HC (n = 48)	p-value
Age (year)	11.73 ± 2.56 (6–18)	11.71 ± 2.95 (6–18)	.9734 ^a
Gender	42/6 (M/F)	39/9 (M/F)	.3991 ^b
Mean FD	0.16 ± 0.07	0.12 ± 0.04	.0028 ^a
FIQ	106.83 ± 17.79	113.81 ± 13.32	.0323 ^a
PIQ	109.48 ± 19.29	110.38 ± 14.59	.7980 ^a
VIQ	103.40 ± 15.50	113.94 ± 12.13	.0004 ^a
ADI-R			
Social score	20.09 ± 5.11 (n = 45)	—	—
Communication score	15.76 ± 4.01 (n = 46)	—	—
RRB score	6.02 ± 2.65 (n = 46)	—	—
ADOS			
Social score	8.06 ± 9.96	—	—
Communication score	3.46 ± 1.65	—	—
Total score	11.52 ± 4.24	—	—
RRB score	2.73 ± 1.54	—	—

Note: Values shown are: mean ± SD.

Abbreviations: ADI-R, Autism Diagnostic Interview-Revised; ADOS, Autism Diagnostic Observation Schedule; FD, framewise displacement; FIQ, Full-Scale Intelligence Quotient; PIQ, Performance Intelligence Quotient; RRB score, Restricted, Repetitive and Stereotyped Behaviors; VIQ, Verbal Intelligence Quotient.

^ap value was obtained by two-sample t-test, two-tailed.

^bp value was obtained by chi-square test, two-tailed.

anti-correlation (Murphy et al., 2009; Murphy & Fox, 2017). We thus did not perform GSR in the current study. Finally, bandpass filtering (0.01–0.08 Hz) was performed to reduce the influence of high-frequency noise (He et al., 2020).

2.4 | Analysis procedure

Figure 1 shows the data analysis process. We first extracted the time series of the regions of interest (ROIs) within the DMN. Then, using the Liang information flow method, we constructed the DMN causal connectivity networks for ASDs and HCs. To better understand the causal connectivity pattern of DMN, we further calculated the network topology properties for the two groups. After that, we compared the causal connectivity differences between the two groups and revealed the relationships between the connectivity with significant differences and clinical symptoms of ASD. Finally, the obtained causal connectivity and network properties were used to construct a classification model to classify the two groups. The details of these steps are described in the following sections.

2.5 | Regions of interest

Inspired by previous studies (Andrews-Hanna et al., 2010; Bathelt & Geurts, 2021; Du et al., 2016), 11 ROIs were selected, which are crucial regions of the DMN. The DMN can be mainly divided into three parts, namely, the midline core including the PCC and aMPFC, the dMPFC subsystem, including the dMPFC, TPJ, LTC, and TempP, and the MTL subsystem, including the vMPFC, pIPL, Rsp, PHC, and HF. According to previous studies (Andrews-Hanna et al., 2010; Du et al., 2016), only the left and middle areas were used in our study to prevent a strong correlation between mirror structures. The ROIs were defined as a sphere with a radius of 6 mm centered on the

corresponding MNI coordinate. The MNI coordinates for these 11 ROIs are listed in Table 2. After that, we extracted the averaged time series signals for each ROI across subjects. These time series were used for calculating the causal connectivity network.

2.6 | Construction of the causal network of the DMN

This study used the unnormalized multivariate Liang information flow analysis proposed by Liang et al. (2021) to construct the causal connectivity network of the DMN. For each subject, we obtained an 11×11 directed causal connectivity matrix. For these directed causal connectivity matrices, we first used the built-in test method in the Liang information flow to test the statistical significance of the causal

TABLE 2 Montreal Neurological Institute (MNI) coordinates of 11 ROIs within DMN

Brain regions	MNI coordinates		
	x	y	z
Posterior cingulate cortex (PCC)	−8	−56	26
Anterior medial prefrontal cortex (aMPFC)	−6	52	−2
Dorsal medial prefrontal cortex (dMPFC)	0	52	26
Temporo-parietal junction (TPJ)	−54	−54	28
Lateral temporal cortex (LTC)	−60	−24	−18
Temporal pole (TempP)	−50	14	−40
Ventral medial prefrontal cortex (vMPFC)	0	26	−18
Posterior inferior parietal lobule (pIPL)	−44	−74	32
Retrosplenial cortex (Rsp)	−14	−52	8
Parahippocampal cortex (PHC)	−28	−40	−12
Hippocampal formation (HF)	−22	−20	−26

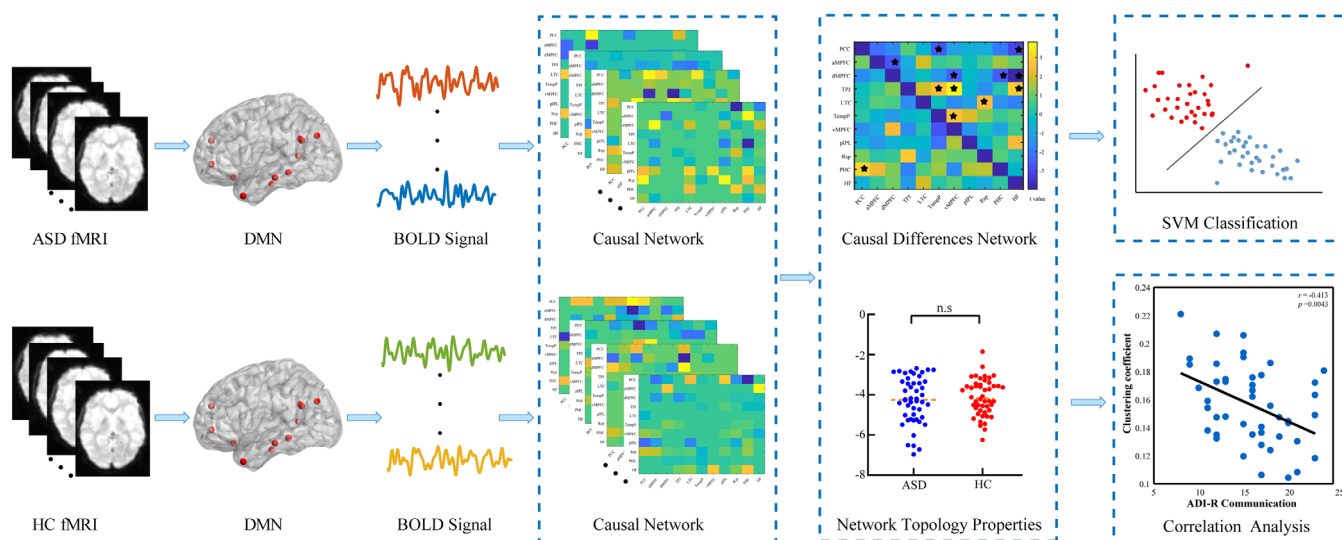


FIGURE 1 The analysis procedure.

matrix, and the details are listed in Section Liang information flow analysis. We set the confidence level at 90% and considered the causal connectivity that failed the significance test to be spurious causal relation, which we hereafter set to zero. After that, we performed the z-score on the causal connectivity matrices to remove the physical units (Abdi, 2007). Subsequently, we regressed the mean FD (Chen et al., 2016) across subjects to further reduce the impact of head motion. The new sparse causality connectivity matrices were used for the following analysis. Finally, we calculated the group-averaged causal connectivity matrix for the ASDs and HCs. We also calculated the distance of the mean causal matrix between ASD and HC using Pearson's correlation (Benesty et al., 2009) to assess the similarity of the causal network architecture. The Liang information flow method will be further introduced below.

2.7 | Liang information flow analysis

Information flow is a real concept in general physics and system dynamics, it is only vaguely studied in a loose sense without a formal expression (Liang & Kleeman, 2005). Motivated by a finding by Liang and Kleeman (2005), Liang (2016b) was able to put information flow on a rigorous footing and establish the whole formalism from the first principles. A particular feature is the natural embedding of causality within formalism, thanks to a proven theorem on causality. This is in contrast to the previous studies where “information flow” and causality are unrelated because of the inappropriate ways to define information flow (Lizier & Prokopenko, 2010).

Recently, Liang conducted a maximum likelihood estimation (MLE) for the result in Liang (2016b), providing a very concise formula for quantitative causal discovery, which can effectively capture the causal relation among time series (Liang, 2014, 2021). This explicitly obtained expression is very concise, involving only sample covariance (Liang, 2014, 2021). In the following, we only list the final result; for a brief description of the theory, please refer to Liang et al. (2021), section 2.

For a vector of state variables $\mathbf{X}=(X_1,\dots,X_d)$, consider a d -dimensional continuous-time stochastic system

$$d\mathbf{X}=\mathbf{F}(\mathbf{X},t)dt+\mathbf{B}(\mathbf{X},t)d\mathbf{W}, \tag{1}$$

where $\mathbf{F}=(F_1,F_2,\dots,F_d)$ may be arbitrary nonlinear differentiable functions of \mathbf{X} and t , \mathbf{W} is a vector of standard Wiener processes, and $\mathbf{B}=(b_{ij})_{d\times m}$ is the matrix of perturbation amplitudes which may also be any differentiable functions of \mathbf{X} and t . Liang (2016b) established that the rate of information flowing from X_j to X_i is (in nats per unit time) is:

$$T_{j\rightarrow i}=-E\left(\frac{1}{\rho_i}\int_{\mathbb{R}^{d-2}}\frac{\partial F_{ij}\rho_j}{\partial X_i}dx_{ij}\right)+\frac{1}{2}E\left(\frac{1}{\rho_i}\int_{\mathbb{R}^{d-2}}\frac{\partial^2(g_{ii}\rho_j)}{\partial X_i^2}dx_{ij}\right), \tag{2}$$

where dx_{ij} signifies $dx_1\dots dx_{i-1}dx_{i+1}\dots dx_{j-1}dx_{j+1}\dots dx_d$, E stands for mathematical expectation, $g_{ii}=\sum_{k=1}^2b_{ik}b_{ik}$, $\rho_i=\rho_i(X_i)$ is the marginal pdf of X_i , and $\rho_j=\int_{\mathbb{R}}\rho(X)dx_j$. Theoretically, if $T_{j\rightarrow i}$ is not zero, then X_j is cause to X_i , and its magnitude measures the size of the causality;

otherwise, it is not causal. Of course, in real applications, a significance test must be performed.

The above formula is exact. It is, however, impossible to calculate the expectations if the joint probability distribution is not known. Liang et al. (2021) later on made a maximum likelihood estimation and found that the rate of Liang information flowing from X_2 to X_1 can be estimated as follows: (in nats per unit time) is

$$\hat{T}_{2\rightarrow 1}=\frac{1}{\det\mathbf{C}}\cdot\sum_{j=1}^d\Delta_{2j}C_{j,d1}\cdot\frac{C_{12}}{C_{11}}, \tag{3}$$

where C_{ij} denotes the sample covariance between X_i and X_j , $C_{j,d1}$ is the sample covariance between X_j and the derived series \dot{X}_1 , $\dot{X}_1=\left\{\dot{X}_{i,n}\right\}$ is the Euler forward differencing approximation of $\frac{dX_1}{dt}$: $\dot{X}_{i,n}=\frac{X_{i,n+k}-X_{i,n}}{k\Delta t}$, $k\Delta t$ is the time interval between $X_{i,n+k}$ and $X_{i,n}$. To ensure accuracy, usually $k=1$. Δ_{ij} represents the cofactors of the matrix $\mathbf{C}=(C_{ij})$.

The T value obtained must be tested for significance. We can use the Fisher information matrix to simplify the problem. According to the property of maximum likelihood estimation, $\hat{T}_{2\rightarrow 1}$ was approximately normally distributed near its true value with a variance $\left(\frac{C_{12}}{C_{11}}\right)^2\hat{\sigma}_{a_{12}}^2$. Here $\hat{\sigma}_{a_{12}}^2$ is the variance of \hat{a}_{12} , which is estimated as follows. Denote $\theta=(f_1,a_{11},a_{12},\dots,a_{1d},b_1)$, the Fisher information matrix can be calculated $\mathbf{I}=(I_{ij})$,

$$I_{ij}=-\frac{1}{N}\sum_{n=1}^N\frac{\partial^2\log\rho(\mathbf{X}_{n+1}|\mathbf{X}_n;\hat{\theta})}{\partial\theta_i\partial\theta_j}. \tag{4}$$

The inverse $(\mathbf{NI})^{-1}$ is the covariance matrix of $\hat{\theta}$, from which can be found \hat{a}_{12} . Given a significance level the confidence interval can be easily found.

2.8 | Granger causality analysis

In 1969, Granger introduced the concept of GCA, that is, if X_2 is known to help predict the future of X_1 , then X_2 “causes” X_1 (Granger, 1969). In this article, we used the conditional Granger causality connectivity to calculate the causal connectivity through the “Granger causal connectivity analysis” (GCCA) toolbox (Seth, 2010).

To illustrate conditional Granger causality analysis, consider time series X_t , Y_t , and Z_t . First, let the joint autoregressive representation of X_t and Z_t be (Ding et al., 2006)

$$\begin{aligned} X_t &= \sum_{j=1}^{\infty} a_{1j}X_{t-j} + \sum_{j=1}^{\infty} b_{1j}Z_{t-j} + \varepsilon_{1t}, \\ Z_t &= \sum_{j=1}^{\infty} c_{1j}X_{t-j} + \sum_{j=1}^{\infty} d_{1j}Z_{t-j} + \gamma_{1t}, \end{aligned} \tag{5}$$

where the covariance matrix of the noise terms is as follows:

$$\Sigma_1=\begin{pmatrix} \Lambda_1 & T_1 \\ T_1 & \Gamma_1 \end{pmatrix}. \tag{6}$$

Then consider the joint autoregressive representation of all three processes X_t , Y_t , and Z_t

$$\begin{aligned} X_t &= \sum_{j=1}^{\infty} a_{2j} X_{t-j} + \sum_{j=1}^{\infty} b_{2j} Y_{t-j} + \sum_{j=1}^{\infty} c_{2j} Z_{t-j} + \varepsilon_{2t}, \\ Y_t &= \sum_{j=1}^{\infty} d_{2j} X_{t-j} + \sum_{j=1}^{\infty} e_{2j} Y_{t-j} + \sum_{j=1}^{\infty} f_{2j} Z_{t-j} + \eta_{2t}, \\ Z_t &= \sum_{j=1}^{\infty} u_{2j} X_{t-j} + \sum_{j=1}^{\infty} v_{2j} Y_{t-j} + \sum_{j=1}^{\infty} w_{2j} Z_{t-j} + \gamma_{2t}, \end{aligned} \quad (7)$$

where the covariance matrix of the noise terms is

$$\Sigma_4 = \begin{pmatrix} \Gamma_{XX} & \Gamma_{XY} & \Gamma_{XZ} \\ \Gamma_{YX} & \Gamma_{YY} & \Gamma_{YZ} \\ \Gamma_{ZX} & \Gamma_{ZY} & \Gamma_{ZZ} \end{pmatrix}. \quad (8)$$

So the Granger causality from Y_t to X_t conditional on Z_t can be defined as

$$F_{Y \rightarrow X|Z} = \ln \frac{\Lambda_1}{\Gamma_{XX}} \quad (9)$$

Therefore, $F_{Y \rightarrow X|Z} = 0$ meaning that no further improvement in the prediction of X_t can be expected by including past measurements of Y_t (Ding et al., 2006). And when there is still a direct component from Y_t to X_t , the inclusion of past measurements of Y_t in addition to that of X_t and Z_t results in better predictions of X_t , which may lead to $\Gamma_{XX} < \Lambda_1$, and $F_{Y \rightarrow X|Z} > 0$ (Ding et al., 2006).

2.9 | Network topology properties

To further explore the DMN causal network patterns, we calculated five common directed network topology properties, including characteristic path length (CPL), clustering coefficient (CC), global efficiency (GE), local efficiency (LE), and In-Out degree (D_{in-out}). The Brain Connectivity Toolbox (Bullmore & Sporns, 2009; Rubinov & Sporns, 2010) (<https://www.nitrc.org/projects/bct/>) was used to calculate the network properties for each subject. During the calculation, the causality matrices were first changed into their absolute values. Then, a weighted and directed matrix (causal matrix) was applied to calculate the topological network properties for each subject. These topological network properties can be defined as,

$$CPL^{\rightarrow} = \frac{1}{n} \sum_{i \in N} \frac{\sum_{j \in N, j \neq i} d_{ij}^{\rightarrow}}{n-1} \quad (10)$$

$$CC^{\rightarrow} = \frac{1}{n} \sum_{i \in N} \frac{\frac{1}{2} \sum_{j, h \in N} (a_{ij} + a_{ji})(a_{ih} + a_{hi})(a_{jh} + a_{hj})}{(k_i^{out} + k_i^{in})(k_i^{out} + k_i^{in} - 1) - 2 \sum_{j \in N} a_{ij} a_{ji}} \quad (11)$$

$$GE^{\rightarrow} = \frac{1}{n} \sum_{i \in N} \frac{\sum_{j \in N, j \neq i} (d_{ij}^{\rightarrow})^{-1}}{n-1} \quad (12)$$

$$LE^{\rightarrow} = \frac{1}{2n} \sum_{i \in N} \frac{\sum_{j, h \in N, j \neq i} (a_{ij} + a_{ji})(a_{ih} + a_{hi}) \left([d_{jh}^{\rightarrow}(N_i)]^{-1} + [d_{hj}^{\rightarrow}(N_i)]^{-1} \right)}{(k_i^{out} + k_i^{in})(k_i^{out} + k_i^{in} - 1) - 2 \sum_{j \in N} a_{ij} a_{ji}} \quad (13)$$

$$D_{in-out} = k_i^{in} - k_i^{out} \quad (14)$$

where a_{ij} is the connection strength from nodes i to j , d_{ij}^{\rightarrow} is the shortest directed path length from nodes i to j , $d_{ij}^{\rightarrow} = \sum_{a_{ij} \in g_{i \rightarrow j}} a_{ij}$, where $g_{i \rightarrow j}$ is the directed shortest path from node i to j . k_i^{out} is the out degree of node i , $k_i^{out} = \sum_{j \in N} a_{ij}$, k_i^{in} is the in-degree of node i , $k_i^{in} = \sum_{j \in N} a_{ji}$, n is the total node number of the current network. N is the number of the set of network nodes.

In addition, the In-Out degrees of the nodes were calculated to evaluate the causal source and target (Gao et al., 2011; Jiao et al., 2011). Nodes with positive In-Out degrees are considered causal targets, and the nodes with negative In-Out degrees are considered causal sources.

2.10 | Identification of the ASD patients based on DMN causal connectivity patterns

Based on the casual connectivity and network properties, we attempted to identify ASD patients from the HCs. We first extracted causal connectivity and network topology properties indexes as features for each subject. Then, a 121-dimensional causal connectivity and a 15-dimensional network property features were obtained and used for classification. These features are normalized to -1 and 1 . Given that several features are uninformative or redundant for classification, reducing the number of features can improve performance (Dosenbach et al., 2010). F score method (Liu et al., 2015; Zhang et al., 2019) was used to select features to improve the classification performance. In this study, support vector machine (SVM) classifier with linear kernel was used (Chang & Lin, 2011). To evaluate the performance of classifier, a leave-one-out cross-validation (LOOCV) strategy was performed. In the linear kernel SVM, only parameter C (penalty coefficient) takes the default value (i.e., $C = 1$).

2.11 | Statistical analysis

We used two-sample t-tests (two-tailed) to compare the causal connectivity and network properties differences in DMN for two groups. For the causal connectivity difference, the significant difference level was set at $p < .05$ (p FDR corrected [Storey, 2002]). For the network property difference, the significant difference level was set at $p < .05$. Pearson's correlation coefficient (Benesty et al., 2009) was used to assess the relationships between causality relations and the clinical symptom of ASD (i.e., ADOS and ADI scores), where the correlation was considered significant when $p < .05$.

3 | RESULTS

3.1 | Between-group DMN causal connectivity difference

GCA and Liang information flow are both popular causal analysis methods. Currently, the GCA is widely used in brain science, while Liang information flow method is commonly used in atmospheric science. In our study, we compared the causal connectivity patterns of DMN for ASD patients and HC using the Liang information flow (Figure 2a–d) and GCA (Figure 2e–h), respectively. For the GCA, we used the Akaike Information Criterion (AIC) and the Bayesian information criterion (BIC) to identify the AR order, the AR order was 10. Figure 2a,b,e,f show the group-averaged causal connectivity of DMN using the Liang information flow and GCA in ASD and HC, respectively. We found the causal network architecture of the DMN is different between the two groups, where the correlation is 0.4239 and 0.3565 for Liang information flow and GCA.

For the Liang information flow, to compare the causal connectivity difference of the DMN between ASD and HC, we performed a two-sample *t*-test (*p*FDR, *p* < .05) on individual DMN causal connectivity matrices. Figure 2c,d display the causal connectivity differences of DMN between the two groups. Compared with the HC group, we found the causal connections in PCC → TempP, PCC → HF, aMPFC → dMPFC, dMPFC → vMPFC, dMPFC → PHC, and dMPFC → HF were significantly decreased in the ASD group. In contrast, the causal connections in the TPJ → TempP, TPJ → vMPFC, TPJ → HF, LTC → Rsp, TempP → vMPFC, and PHC → PCC were significantly increased in ASD. We also found that the PCC, dMPFC, TPJ, vMPFC, TempP, and HF produce more causal connectivity differences.

For the GCA, we also performed a two-sample *t*-test (*p*FDR, *p* < 0.05) on individual DMN causal connectivity matrices for the two groups. Figure 2g,h show the causal connectivity difference of DMN between ASD and HC. Compared with the HC group, we found the causal connections in dMPFC → PCC, TempP → PCC, TPJ → LTC, LTC → TPJ, pIPL → LTC, vMPFC → HF, pIPL → TempP, and pIPL → Rsp were significantly decreased in ASD, while the causal connections in aMPFC → Rsp, dMPFC → TPJ, dMPFC → Rsp, TPJ → TempP, PHC → Rsp, and HF → PCC were significantly increased in ASD. In addition, we found the dMPFC, PCC, TPJ, Rsp, and pIPL produce more causal connectivity differences.

The DMN causal connectivity differences based on both methods involve the dMPFC and MTL subsystems. The main difference between the two approaches is that the causal connectivity across vMPFC obtained by Liang information flow shows more difference, while GCA has no significant causal difference. In addition, compared with the GCA, we found that the causal connectivity difference shows a hierarchical regulation model using Liang information flow, which could provide a novel perspective for understanding the DMN causal connectivity pattern in ASD.

3.2 | Between-group DMN network topological properties difference

To better investigate the causal connectivity network patterns, we calculated the network properties for each subject and compared network properties differences between ASD and HC. Figure 3a shows the between-group DMN network properties difference. We found significant differences in the clustering coefficient, while there were no significant differences in the characteristic path length, global efficiency, and local efficiency. We also found that the node aMPFC has significant differences (*p* = .0159) in In-Out degree between ASD and HC.

The mean In-Out degree of the nodes in the DMN is listed in Figure 3b. For the two groups, we consistently found that the In-Out degree of the TPJ, TempP, vMPFC, Rsp, and HF was >0 and they act as a causal target, while the In-Out degree of the PCC, aMPFC, pIPL, and PHC were <0 and they act as a causal source. In particular, we found that the causal directions of the dMPFC and LTC were opposite between ASD and HC.

3.3 | Relationships between DMN causal network patterns and ASD symptoms

Figure 4 shows the correlations between the DMN causal network patterns and the clinical symptoms of ASD. For the causal connectivity, we found that the causal connectivity from dMPFC to vMPFC within DMN was negatively correlated with the ADOS social score (*r* = −.375, *p* = .0087), ADOS communication score (*r* = −.404, *p* = .0044), and ADOS total score (*r* = −.418, *p* = .0031). The causal connectivity from dMPFC to PHC was positively correlated with the ADOS communication score (*r* = .371, *p* = .0095), the causal connectivity from dMPFC to HF was negatively correlated with the ADOS communication score (*r* = −.287, *p* = .0480). For the network properties, we found that the clustering coefficient of the DMN was negatively correlated with the ADI-R communication scores (*r* = −.413, *p* = .0043).

3.4 | Classification of the two groups

We used the causal connectivity and network properties of the DMN as features to construct a classification model. Table 3 shows the classification results of SVM using the *F*-score method in the different feature selection conditions. The highest classification accuracy (78.12%) was obtained based on the combination of causal connectivity and network properties.

4 | DISCUSSION

To the best of our knowledge, this is the first study to apply the Liang causal information flow method to fMRI data to explore the resting

The Liang information flow results

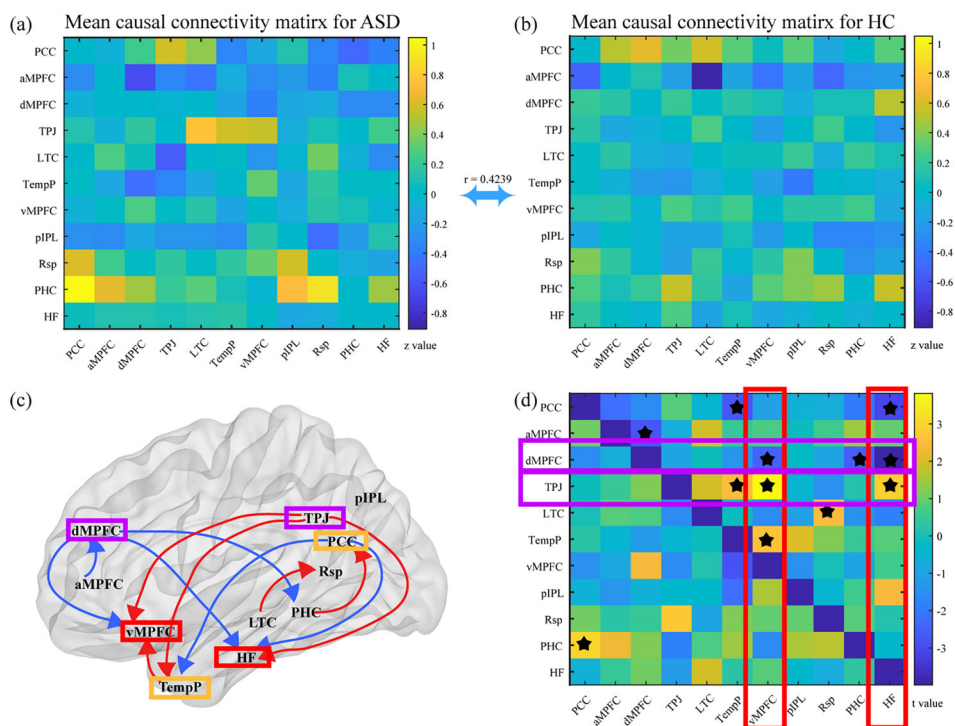
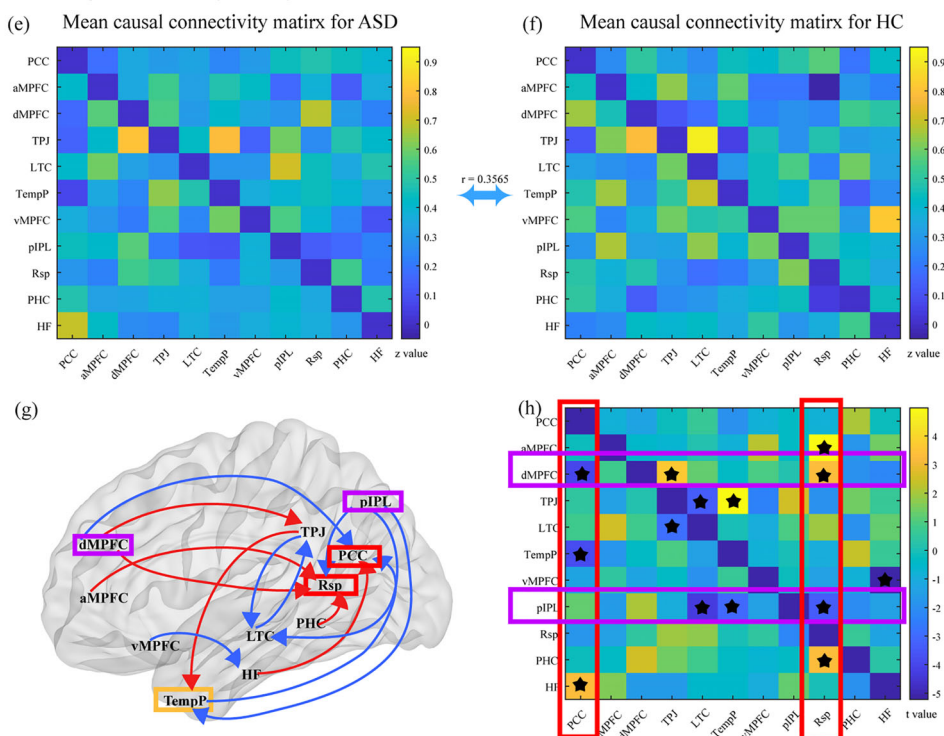


FIGURE 2 The mean causal connectivity patterns of DMN for ASD and HC groups were constructed by Liang information flow (a and b) and GCA (e and f), respectively. (c) The causal connectivity differences between the HC group and the ASD group ($pFDR p < .05$) were obtained using Liang information flow. (d) Causal connectivity differences t -values map. (g) The causal connectivity differences between the HC group and the ASD group ($pFDR p < .05$) were obtained using GCA. (h) Causal connectivity differences t -values map. The blue edges represent decreased causal connectivity. The red edges represent increased causal connectivity. The area marked with a star indicates a significant causal connectivity difference.

The Granger causality analysis results



DMN inter-regional causal connectivity patterns in ASD. Based on the seed method, we constructed the DMN causal connectivity network and calculated the network topology properties. Compared with HC, we observed that the interactions among the PCC, dMPFC, TPJ, TempP, vMPFC, and HF showed more inter-regional causal

connectivity differences in ASD. The network clustering coefficient and the In-Out degrees of aMPFC were significantly decreased in ASD. Moreover, these DMN causal connectivity network patterns, especially the causal connections from dMPFC to vMPFC, PHC, and HF, were correlated with the clinical symptoms (i.e., ADOS social,

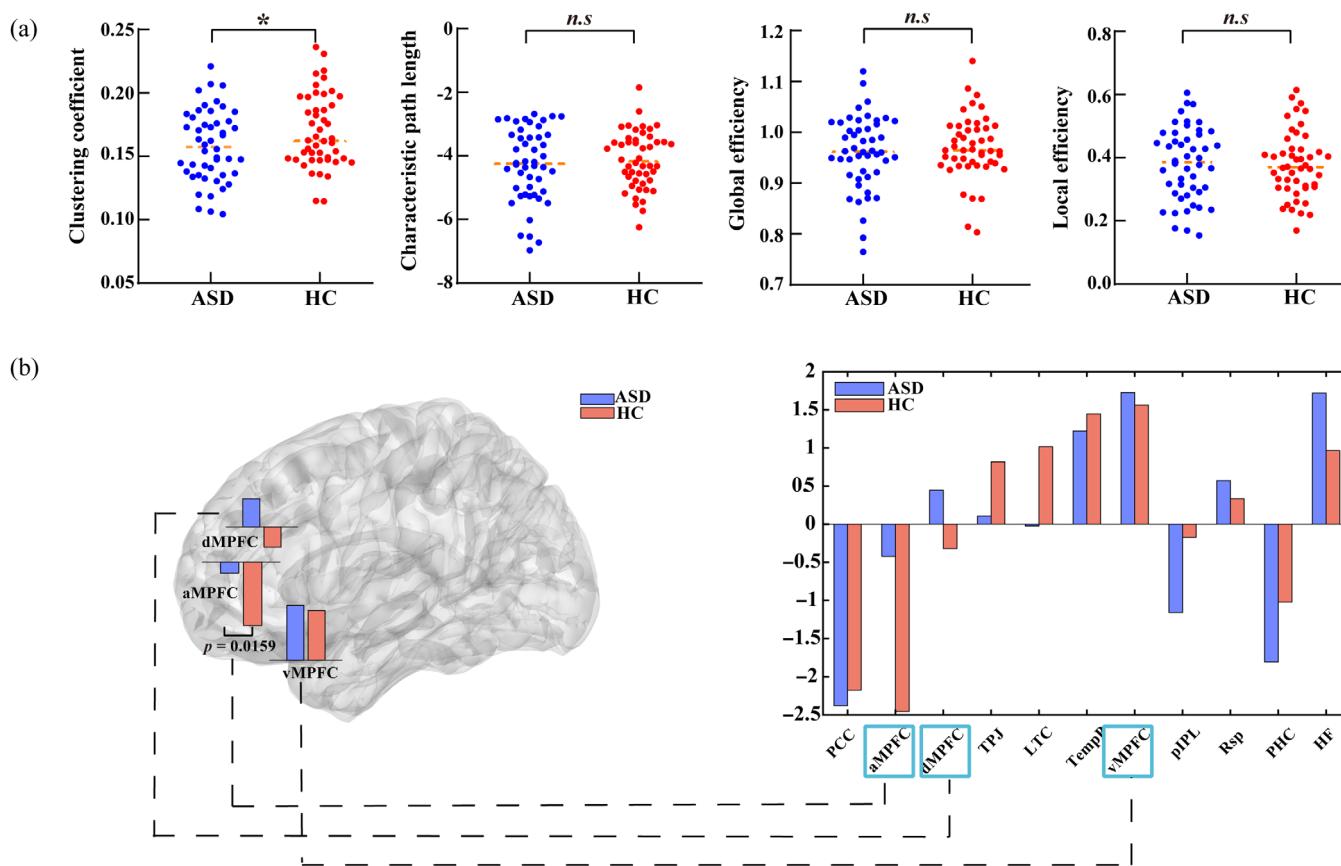


FIGURE 3 (a) The differences in four network properties between the two groups. The star represents the significant differences, where $p < .05$. (b) The mean In-Out degrees of the nodes in the ASD and HC group. The negative values represent the node as the causal source, and positive values represent the node as the causal target.

ADOS total, and ADOS communication) of ASD and can be important features to identify ASD. Our findings highlight the utility of the Liang information flow method in brain causal network analysis and verify that altered inter-DMN causal connectivity patterns are associated with social deficits in ASD.

4.1 | Methodological considerations

In terms of methodology, GCA and Liang information flow are both commonly used time series causality analysis tools (McCracken, 2016). GCA is a method that relies on models of the time series data for causal inference, that is, multivariate autoregressive (MVAR). However, several previous studies have indicated that the MVAR-based causal model only considered the lag relation between time series, whereas the instantaneous effect is ignored (Faes et al., 2013; Salehi et al., 2022). In addition, Granger himself also pointed out that GCA may not necessarily a true causal relation (Granger, 1963). Compared with GCA, since the Liang information flow method is rigorously established from first principles, it does not require assumptions and may be able to capture the real causality of brain networks. For this reason, it has been widely used to quantify causal relations in classical systems (Liang, 2016b) and network theory

(Li & Liu, 2019). It has been widely used in finance (Liang, 2016a), climate (Liang et al., 2021), quantum mechanics (Yi & Bose, 2022), and neuroscience (Hristopulos et al., 2019). Particularly, Hristopulos et al. (2019) applied this causal connectivity approach to the EEG time series to study the information flow disruption in a concussed brain, showing that it could effectively construct causal networks for different cognitive activities. Following this, we utilized the Liang information flow method to construct the causal connectivity network from resting-state fMRI, which entailed some interesting results. Furthermore, we also compared the results of the two methods (see Appendix S1). Below we only discuss the results of Liang information flow.

4.2 | Altered causal network architecture of DMN in ASD

The DMN is a higher-order cognitive network that shows substantial overlap with the “social brain” network (Blakemore, 2008). Many studies have reported that abnormal functional network patterns within- and between-DMN were closely associated with social deficits in ASD (Feng et al., 2022; Lynch et al., 2013; Padmanabhan et al., 2017). The FC alteration in DMN could be a potential

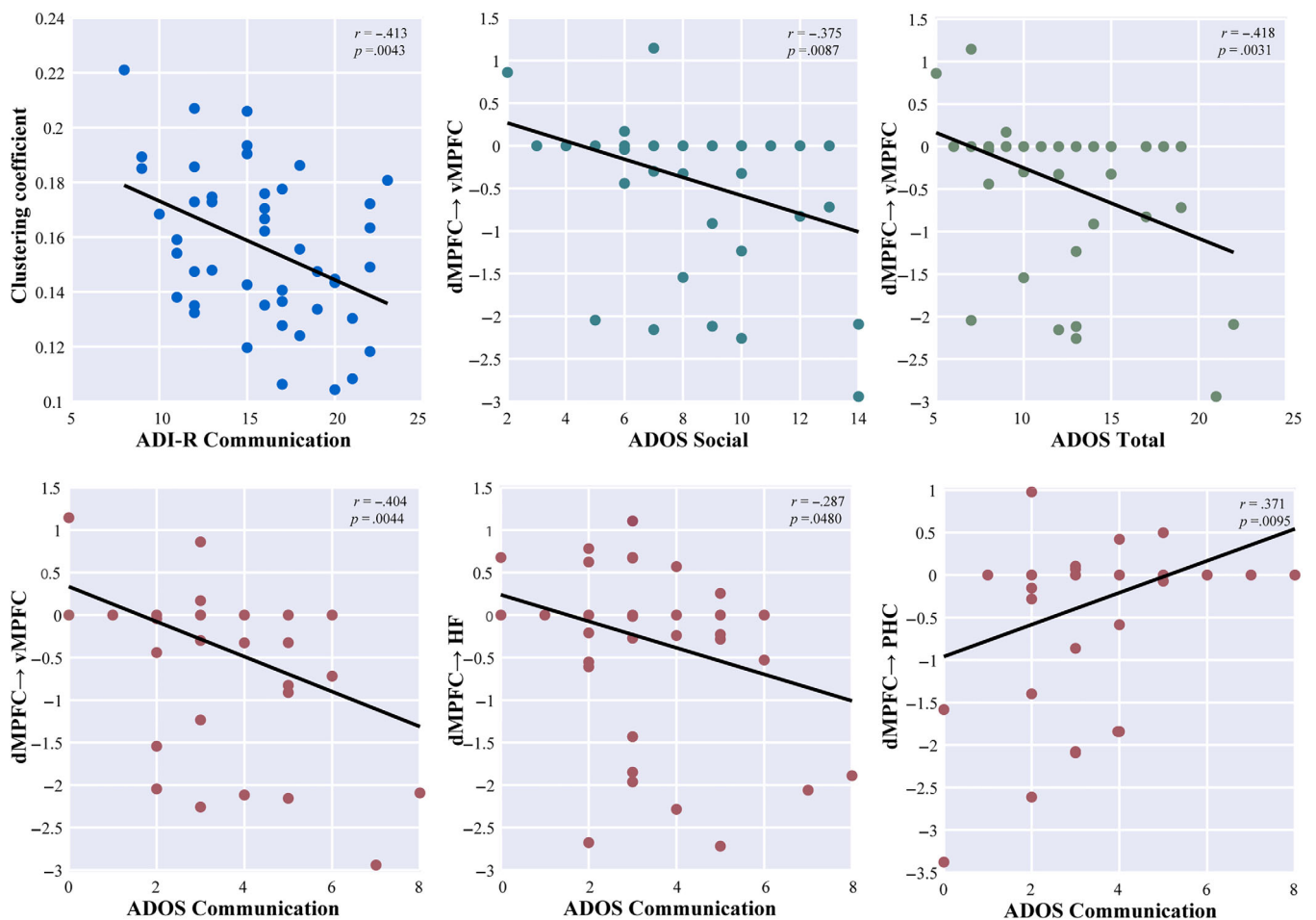


FIGURE 4 The correlation between the difference in causal relations and the behavioral scales of the ASD group.

TABLE 3 Classification results of the SVM using F score based on the DMN causal patterns

	Causal relations differences	Network properties	Network properties and causal relations differences
Accuracy	77.08%	68.75%	78.12%
Sensitivity	73.91%	69.57%	80.43%
Specificity	84.00%	68.00%	80.00%

endophenotype for social deficits in ASD (Feng et al., 2022) because the DMN architecture has an important impact on the information integration of the brain during rest and task performance (Smallwood et al., 2021). Thirty years of brain imaging research have converged to uncover that the DMN is a heterogeneous brain system network that can be further fractionated into multiple dissociated “subsystems” and/or “subnetworks” (Andrews-Hanna et al., 2010). In a previous study conducted by Andrews-Hanna et al. (2010), it was found that the DMN comprises of three dissociated components, including a midline core, a dMPFC subsystem, and a Medial Temporal Lobe (MTL) subsystem.

In addition, our results revealed that, in terms of causal connectivity, ASD patients exhibit significantly reduced strengths from core to another two subsystems (i.e., $PCC \rightarrow TempP$, $PCC \rightarrow HF$, and

$aMPFC \rightarrow dMPFC$) and from dMPFC to MTL subsystem (i.e., $dMPFC \rightarrow vMPFC$, $dMPFC \rightarrow PHC$, and $dMPFC \rightarrow HF$), as well as significantly increased strengths from TPJ to MTL subsystem (i.e., $TPJ \rightarrow vMPFC$ and $TPJ \rightarrow HF$) compared with HC. Furthermore, the excitation-inhibition imbalance of DMN may lead to social impairment (Padmanabhan et al., 2017; Paine et al., 2017; Trakoshis et al., 2020). This finding indicated that the core (PCC and aMPFC) regions exerted less influence on other subsystems. The dMPFC and TPJ are two major regions in the dMPFC subsystem and the vMPFC and HF are two key regions in the MTL subsystem. The causal interaction difference among these four regions indicated that the dMPFC subsystem may act as a mentor to influence on the MTL subsystem, indicating the influence exerted by the dMPFC subsystem on the MTL subsystem may modulate the social function of the DMN. We

also found that the DMN causal connectivity network architecture is relatively dissimilar ($r = .4239$) between ASD and HC compared with previous reported resting-state functional connectivity network (Cole et al., 2014; Schultz & Cole, 2016; Zhang et al., 2019). This finding implied that the resting DMN inter-regional information coupling does not have an “intrinsic” pattern between ASD and HC, whereas exhibiting a disease-related excitation–inhibition imbalance causal network pattern. Thus, we suggested that the Liang information flow causal connectivity analysis could deepen our knowledge of the DMN network architecture and provide a new perspective to enrich our understanding of ASD.

4.3 | Reduced causal connectivity aMPFC → dMPFC and dMPFC → vMPFC

The existing studies have shown that the MPFC is recognized as the key component of the neurocircuitry related to various social cognition (Smallwood et al., 2021). Damage to MPFC impairs the ability to process social information related to oneself (present and future self) in ASD (Guise & Shapiro, 2017; Maggi & Humphries, 2022; Padmanabhan et al., 2017). The MPFC often comprises three functionally dissociable and hierarchically organized subregions: vMPFC, aMPFC, and dMPFC (Gusnard et al., 2001). These three subregions are located in the different subsystems of the DMN, respectively, yet they are functionally inter-connected with each other and play distinct roles in social cognition (Padmanabhan et al., 2017). In our study, we found that the causal connectivity aMPFC → dMPFC and dMPFC → vMPFC were significantly reduced in ASD compared with HC. Previously, Kim (2020) suggested that the distinctive subregions in the MPFC exhibited a hierarchical allostatic regulation model that integrates a wide range of MPFC functions. Such causal connectivity differences may provide new support for the hierarchical connectivity model of MPFC. Using the degree analysis, we also found that the dMPFC acts as a causal information target in ASD, but a causal information source in HC. Compared with HC, ASD patients showed significantly reduced In–Out degree in the aMPFC. The In–Out degree of a node can measure the relative contribution of a node to causality (Jiao et al., 2011). For the causal (effective) connectivity, the decreased causal connectivity may represent a reduction in the influence (inhibits/facilitates) of one region on another, while increased causal connections may represent an increase in the intervention (disruption or promotion) of one region on another (Jiao et al., 2011). These findings may imply that the aMPFC and dMPFC within DMN may be impaired in ASD, indicating weaker influence (directed interaction) of aMPFC on dMPFC and dMPFC on vMPFC.

Furthermore, we found that the causal connectivity dMPFC → vMPFC was significantly negatively correlated with the neuropsychological score (ADOS total, ADOS social, and ADOS communication) of ASD. The higher the ADOS and ADI-R scores, the more severe the ASD symptoms (Lefort-Besnard et al., 2020). This result indicated that the aberrant afferent connection of vMPFC from dMPFC inhibits social behavior in ASD. The dMPFC is a key region of

the dMPFC subsystem of the DMN and is involved in self-reference guidelines or introspective mental activity-related spontaneity, while the vMPFC is a key region of the MTL subsystem of the DMN and is considered for the integration of cognitive and emotional processing (Gusnard & Raichle, 2001). In a previous study conducted by Inagaki and Meyer (2020), they suggested that the greater dMPFC subsystem connectivity at rest was associated with greater social support. Based on the transcranial magnetic stimulation (TMS) study, Ferrari et al. (2016) found that the dMPFC played a causal role in integrating social behaviors. Martin et al. (2017) using focal high-definition transcranial direct current stimulation (HD-tDCS), they demonstrated that the dMPFC played a causal role in integrating higher-order information from others/external sources into that of the self across cognitive domains. In addition, Salehinejad et al. (2021) found that by using anodal tDCS to increase the activation of the vMPFC, the ASD symptoms were significantly reduced. Thus, we suspect that more suppressed from dMPFC to vMPFC may disrupt the social task performance by issuing signals to interfere with the control set maintained by vMPFC.

4.4 | Increased causal connectivity from TPJ to MTL subsystem

TPJ is another hub region in the dMPFC subsystem of DMN. Previous studies have shown that the TPJ plays a crucial role in mediating social cognition (Igelström et al., 2015; Igelström et al., 2017; Kelly et al., 2014) and ToM theory (Chen et al., 2021). It contributes to multisensory integration, a sense of agency, and stimulus-driven attention functions (Eddy, 2016). Several studies also have shown that the lesions of the TPJ may cause ASD (Nobusako et al., 2017). We found that the causal connections from TPJ to MTL subsystem (TPJ → vMPFC, TPJ → HF) were significantly increased, indicating the TPJ exerted more influence on the MTL system. Andrews-Hanna et al. (2010) demonstrated that the dMPFC subsystem is mainly involved in social processing, while the MTL subsystem is mainly involved in memory retrieval. Previous studies have also shown that TPJ is overactivated. For example, Chien et al. (2015) found that the posterior right TPJ was hyperconnected to the right ventral occipitotemporal in ASD boys, and this abnormal hyperconnectivity was related to social behavior. Schulte-Rüther et al. (2011) found increased activation of the right TPJ during self-task in ASD patients. Furthermore, Hadjikhani et al. (2014) found increased activations in the TPJ of ASD during cognitive reappraisal compared with HC. Iidaka et al. (2019) found that the left TPJ was hyperconnected to the bilateral PCC using a large dataset from multiple sites in the ABIDEII. In addition, Eack et al. (2017) found that ASD had significantly enhanced connectivity between left TPJ and the left orbitofrontal cortex and bilateral medial prefrontal cortices compared with HC in the direct comparisons of connectivity strength. This abnormal hyperconnectivity was associated with the pathophysiology of ASD. These findings suggested that the enhanced causal connectivity observed in ASD may imply TPJ dysfunction. Combined with the discussion above, our

results indicated that the excitation–inhibition imbalance (TPJ and dMPFC) within the dMPFC subsystem might lead to disorganized information processing in regional circuitry and potentially reduced sociability.

4.5 | Global causal network topological properties within DMN

In addition to identifying the causal connectivity differences, we also assessed the causal network topographic properties for each subject. The brain network is a usually small-world network that exhibits a large clustering coefficient and a small shortest path length (Bassett & Bullmore, 2006). We found that the global clustering coefficient was significantly lower in ASD compared with HC. However, no significant difference was apparent in characteristic path length, global efficiency, and local efficiency between the two groups. Our finding is in line with previous reports. For example, Rudie et al. (2013) found that the default and higher-order visual regions displayed reduced functional segregation (lower clustering coefficient) in ASD. Based on the EEG network, Barttfeld et al. (2011) also found that the brain network topology of ASD patients departs from small-world behavior, which has less clustering coefficient. The global clustering coefficient is a major measurement of the functional segregation of the whole network (Bullmore & Sporns, 2009; Rubinov & Sporns, 2010). In Yerys's report, they found that the DMN shows a pattern of poor functional segregation in ASD (Yerys et al., 2015). Thus, we suggested that the lower clustering coefficient could cause the loss of small-world of DMN in ASD, affecting the efficiency of information transmission and storage within DMN. Furthermore, we found that higher scores accompanied lower global clustering coefficients. This topological alteration indicated an overall reduced causal segregation (i.e., excitation/inhibition imbalance) of the DMN with increasing ASD severity.

4.6 | Identification of ASD using causal networks

In clinical diagnosis, a challenging problem is the accurate identification of ASD, and there is an urgent need to provide an effective method. Thus, in this study, we used the causal connectivity obtained by Liang information flow to classify ASD from HC. We found that the DMN causal connectivity pattern could be an important feature in identifying ASD (see Table 3), and the combination of features (causal connectivity and network properties) produced a higher classification accuracy than a single feature, achieving a 78.12% accuracy with a linear SVM classifier. Meanwhile, the traditional approach to distinguishing ASD from HC is based on functional connectivity (Hull et al., 2017; Santana et al., 2022). However, cognitive activity or connectivity of the brain is largely determined by the causal influences between brain regions. Figures 2 and 3 show that the changes in causal connectivity and network properties are important for ASD. Therefore, the Liang information flow method could offer a new strategy for the clinical diagnosis of ASD.

5 | LIMITATIONS

There are some limitations in the current study. First, our sample size is relatively small since we only use the data from the NYU site in ABIDE. In addition, although previous studies have shown that the prevalence of ASD in males is ~3 to 4 times higher than in females (Lawrence et al., 2020), the gap between males and females was even greater in our study. Future studies should use multisite data and larger samples to overcome the gender mismatch problem, replication and further exploration. Second, we identified alterations in causal connectivity within the DMN and obtained the brain regions associated with social behaviors, but our study was based on resting-state fMRI data and may not be able to capture real socially relevant processes. Future work should further explore the alteration of network causal connectivity during social tasks. In addition, we should combine TMS/tDCS to verify the causal connectivity results we obtained using the Liang information flow method in future studies.

6 | CONCLUSION

To conclude, we used the Liang causal information flow method to explore the causal interactions within the DMN involving ASD patients. Our findings showed a specific disruption of causal connectivity among the core subsystem, dMPFC subsystem, and MTL subsystem of the DMN in ASD patients. Compared with the HC group, we found that the causal connectivity from the core subsystem to the dMPFC and MTL subsystem ($PCC \rightarrow TempP$, $PCC \rightarrow HF$, and $aMPFC \rightarrow dMPFC$) was significantly decreased in the ASD group. We also found the imbalance inhibits/facilitates interactions from the dMPFC subsystem to the MTL subsystem, such as significantly increased causal connectivity in $dMPFC \rightarrow vMPFC$, $dMPFC \rightarrow PHC$, and $dMPFC \rightarrow HF$, and significantly decreased causal connectivity in $TPJ \rightarrow TempP$, $TPJ \rightarrow vMPFC$, $TPJ \rightarrow HF$, $TempP \rightarrow vMPFC$, and $PHC \rightarrow PCC$. For the topological property analysis, we also found the clustering coefficient of DMN and the In-Out degrees of aMPFC were significantly decreased in ASD. Moreover, these DMN causal connectivity network patterns, especially the causal connections from dMPFC to vMPFC, PHC, and HF, were correlated with the clinical symptoms of ASD and can be important features in identifying ASD. These differences in causal connectivity patterns indicated that the DMN inter-regions information processing or signal issuing was perturbed in ASD, which might contribute to the deficits of social cognition.

ACKNOWLEDGMENTS

This work was supported by grants from the National Natural Science Foundation of China (#62006197, #61961160705, #U19A2082); the Project of Science and Technology Department of Sichuan Province (#2018JY0526).

CONFLICT OF INTEREST

The authors declare no conflict of interest.

DATA AVAILABILITY STATEMENT

Original rs-fMRI data and phenotypes were downloaded from the ABIDE repository (ABIDEs I, http://fcon_1000.projects.nitrc.org/indi/abide/).

ORCID

Jing Cong  <https://orcid.org/0000-0002-2922-9269>

REFERENCES

- Abdi, H. (2007). Z-scores. In N. Salkind (Ed.), *Encyclopedia of measurement and statistics* (Vol. 3, pp. 1055–1058). Sage.
- American Psychiatric Association. (2013). *Diagnostic and statistical manual of mental disorders (DSM-5®)*. American Psychiatric Publishing.
- Andrews-Hanna, J. R., Reidler, J. S., Sepulcre, J., Poulin, R., & Buckner, R. L. (2010). Functional-anatomic fractionation of the brain's default network. *Neuron*, *65*, 550–562.
- Assaf, M., Jagannathan, K., Calhoun, V. D., Miller, L., Stevens, M. C., Sahl, R., O'Boyle, J. G., Schultz, R. T., & Pearlson, G. D. (2010). Abnormal functional connectivity of default mode sub-networks in autism spectrum disorder patients. *NeuroImage*, *53*, 247–256.
- Barttfeld, P., Wicker, B., Cukier, S., Navarta, S., Lew, S., & Sigman, M. (2011). A big-world network in ASD: Dynamical connectivity analysis reflects a deficit in long-range connections and an excess of short-range connections. *Neuropsychologia*, *49*, 254–263.
- Bassett, D. S., & Bullmore, E. (2006). Small-world brain networks. *The Neuroscientist*, *12*, 512–523.
- Bathelt, J., & Geurts, H. M. (2021). Difference in default mode network subsystems in autism across childhood and adolescence. *Autism*, *25*, 556–565.
- Benesty, J., Chen, J., Huang, Y., & Cohen, I. (2009). Pearson correlation coefficient. In I. Cohen (Ed.), *Noise reduction in speech processing* (pp. 1–4). Springer.
- Biswal, B., Zerrin Yetkin, F., Haughton, V. M., & Hyde, J. S. (1995). Functional connectivity in the motor cortex of resting human brain using echo-planar MRI. *Magnetic Resonance in Medicine*, *34*, 537–541.
- Blakemore, S.-J. (2008). The social brain in adolescence. *Nature Reviews Neuroscience*, *9*, 267–277.
- Broyd, S. J., Demanuele, C., Debener, S., Helps, S. K., James, C. J., & Sonuga-Barke, E. J. (2009). Default-mode brain dysfunction in mental disorders: A systematic review. *Neuroscience & Biobehavioral Reviews*, *33*, 279–296.
- Bullmore, E., & Sporns, O. (2009). Complex brain networks: Graph theoretical analysis of structural and functional systems. *Nature Reviews Neuroscience*, *10*, 186–198.
- Chang, C.-C., & Lin, C.-J. (2011). LIBSVM: A library for support vector machines. *ACM Transactions on Intelligent Systems and Technology (TIST)*, *2*, 1–27.
- Chen, H., Uddin, L. Q., Zhang, Y., Duan, X., & Chen, H. (2016). Atypical effective connectivity of thalamo-cortical circuits in autism spectrum disorder. *Autism Research*, *9*, 1183–1190.
- Chen, L., Chen, Y., Zheng, H., Zhang, B., Wang, F., Fang, J., Li, Y., Chen, Q., & Zhang, S. (2021). Changes in the topological organization of the default mode network in autism spectrum disorder. *Brain Imaging and Behavior*, *15*, 1058–1067.
- Cheng, C.-H., & Redfern, S. A. (2022). Impact of interannual and multidecadal trends on methane-climate feedbacks and sensitivity. *Nature Communications*, *13*, 1–11.
- Chien, H. Y., Lin, H. Y., Lai, M. C., Gau, S. S. F., & Tseng, W. Y. I. (2015). Hyperconnectivity of the right posterior temporo-parietal junction predicts social difficulties in boys with autism spectrum disorder. *Autism Research*, *8*, 427–441.
- Cole, M. W., Bassett, D. S., Power, J. D., Braver, T. S., & Petersen, S. E. (2014). Intrinsic and task-evoked network architectures of the human brain. *Neuron*, *83*, 238–251.
- D'Argembeau, A., Collette, F., van der Linden, M., Laureys, S., del Fiore, G., Degueldre, C., Luxen, A., & Salmon, E. (2005). Self-referential reflective activity and its relationship with rest: A PET study. *NeuroImage*, *25*, 616–624.
- Dejman, A., Khadem, A., & Khorrami, A. (2017). *Exploring the disorders of brain effective connectivity network in ASD: A case study using EEG, transfer entropy, and graph theory* (pp. 8–13). IEEE.
- Di Martino, A., Yan, C.-G., Li, Q., Denio, E., Castellanos, F. X., Alaerts, K., Anderson, J. S., Assaf, M., Bookheimer, S. Y., & Dapretto, M. (2014). The autism brain imaging data exchange: Towards a large-scale evaluation of the intrinsic brain architecture in autism. *Molecular Psychiatry*, *19*, 659–667.
- Ding, M., Chen, Y., & Bressler, S. L. (2006). Granger causality: Basic theory and application to neuroscience. In M. Winterhalder, B. Schelter, & J. Timmer (Eds.), *Handbook of time series analysis: recent theoretical developments and applications* (pp. 437–460). Wiley.
- Docquier, D., Vannitsem, S., Ragone, F., Wyser, K., & Liang, X. S. (2022). Causal links between Arctic sea ice and its potential drivers based on the rate of information transfer. *Geophysical Research Letters*, *49*, e2021GL095892.
- Dosenbach, N. U., Nardos, B., Cohen, A. L., Fair, D. A., Power, J. D., Church, J. A., Nelson, S. M., Wig, G. S., Vogel, A. C., & Lessov-Schlaggar, C. N. (2010). Prediction of individual brain maturity using fMRI. *Science*, *329*, 1358–1361.
- Du, Y., Pearlson, G. D., Yu, Q., He, H., Lin, D., Sui, J., Wu, L., & Calhoun, V. D. (2016). Interaction among subsystems within default mode network diminished in schizophrenia patients: A dynamic connectivity approach. *Schizophrenia Research*, *170*, 55–65.
- Eack, S. M., Wojtalik, J. A., Keshavan, M. S., & Minshew, N. J. (2017). Social-cognitive brain function and connectivity during visual perspective-taking in autism and schizophrenia. *Schizophrenia Research*, *183*, 102–109.
- Eddy, C. M. (2016). The junction between self and other? Temporo-parietal dysfunction in neuropsychiatry. *Neuropsychologia*, *89*, 465–477.
- Faes, L., Erla, S., Porta, A., & Nollo, G. (2013). A framework for assessing frequency domain causality in physiological time series with instantaneous effects. *Philosophical Transactions of the Royal Society A: Mathematical, Physical and Engineering Sciences*, *371*, 20110618.
- Feng, Y., Kang, X., Wang, H., Cong, J., Zhuang, W., Xue, K., Li, F., Yao, D., Xu, P., & Zhang, T. (2022). The relationships between dynamic resting-state networks and social behavior in autism spectrum disorder revealed by fuzzy entropy-based temporal variability analysis of large-scale network. *Cerebral Cortex*, *03*, 1–13.
- Ferrari, C., Lega, C., Vernice, M., Tamietto, M., Mende-Siedlecki, P., Vecchi, T., Todorov, A., & Cattaneo, Z. (2016). The dorsomedial prefrontal cortex plays a causal role in integrating social impressions from faces and verbal descriptions. *Cerebral Cortex*, *26*, 156–165.
- Gao, Q., Duan, X., & Chen, H. (2011). Evaluation of effective connectivity of motor areas during motor imagery and execution using conditional Granger causality. *NeuroImage*, *54*, 1280–1288.
- Granger, C. W. (1969). Investigating causal relations by econometric models and cross-spectral methods. *Econometrica*, *37*, 424–438.
- Granger, C. W. J. (1963). Economic processes involving feedback. *Information and Control*, *6*, 28–48.
- Guise, K. G., & Shapiro, M. L. (2017). Medial prefrontal cortex reduces memory interference by modifying hippocampal encoding. *Neuron*, *94*, 183–192.
- Gusnard, D. A., Akbudak, E., Shulman, G. L., & Raichle, M. E. (2001). Medial prefrontal cortex and self-referential mental activity: Relation to a default mode of brain function. *Proceedings of the National Academy of Sciences*, *98*, 4259–4264.
- Gusnard, D. A., & Raichle, M. E. (2001). Searching for a baseline: Functional imaging and the resting human brain. *Nature Reviews Neuroscience*, *2*, 685–694.
- Hadjikhani, N., Zürcher, N. R., Rogier, O., Hippolyte, L., Lemonnier, E., Ruest, T., Ward, N., Lassalle, A., Gillberg, N., & Billstedt, E. (2014).

- Emotional contagion for pain is intact in autism spectrum disorders. *Translational Psychiatry*, 4, e343.
- Harmah, D. J., Li, C., Li, F., Liao, Y., Wang, J., Ayedh, W., Bore, J. C., Yao, D., Dong, W., & Xu, P. (2020). Measuring the non-linear directed information flow in schizophrenia by multivariate transfer entropy. *Frontiers in Computational Neuroscience*, 13, 85.
- He, C., Chen, H., Uddin, L. Q., Erramuzpe, A., Bonifazi, P., Guo, X., Xiao, J., Chen, H., Huang, X., & Li, L. (2020). Structure-function connectomics reveals aberrant developmental trajectory occurring at preadolescence in the autistic brain. *Cerebral Cortex*, 30, 5028–5037.
- Hlaváčková-Schindler, K., Paluš, M., Vejmelka, M., & Bhattacharya, J. (2007). Causality detection based on information-theoretic approaches in time series analysis. *Physics Reports*, 441, 1–46.
- Hristopoulos, D. T., Babul, A., Babul, S. A., Brucar, L. R., & Virji-Babul, N. (2019). Disrupted information flow in resting-state in adolescents with sports related concussion. *Frontiers in Human Neuroscience*, 13, 419.
- Hull, J. V., Dokovna, L. B., Jacokes, Z. J., Torgerson, C. M., Irimia, A., & Van Horn, J. D. (2017). Resting-state functional connectivity in autism spectrum disorders: A review. *Frontiers in Psychiatry*, 7, 205.
- Igelström, K. M., Webb, T. W., & Graziano, M. S. (2015). Neural processes in the human temporoparietal cortex separated by localized independent component analysis. *Journal of Neuroscience*, 35, 9432–9445.
- Igelström, K. M., Webb, T. W., & Graziano, M. S. (2017). Functional connectivity between the temporoparietal cortex and cerebellum in autism spectrum disorder. *Cerebral Cortex*, 27, 2617–2627.
- Iidaka, T., Kogata, T., Mano, Y., & Komeda, H. (2019). Thalamocortical hyperconnectivity and amygdala-cortical hypoconnectivity in male patients with autism spectrum disorder. *Frontiers in Psychiatry*, 10, 252.
- Inagaki, T. K., & Meyer, M. L. (2020). Individual differences in resting-state connectivity and giving social support: Implications for health. *Social Cognitive and Affective Neuroscience*, 15, 1076–1085.
- Jiao, Q., Lu, G., Zhang, Z., Zhong, Y., Wang, Z., Guo, Y., Li, K., Ding, M., & Liu, Y. (2011). Granger causal influence predicts BOLD activity levels in the default mode network. *Human Brain Mapping*, 32, 154–161.
- Kamiński, M., Ding, M., Truccolo, W. A., & Bressler, S. L. (2001). Evaluating causal relations in neural systems: Granger causality, directed transfer function and statistical assessment of significance. *Biological Cybernetics*, 85, 145–157.
- Kelly, Y. T., Webb, T. W., Meier, J. D., Arcaro, M. J., & Graziano, M. S. (2014). Attributing awareness to oneself and to others. *Proceedings of the National Academy of Sciences*, 111, 5012–5017.
- Kim, H. (2020). Stability or plasticity?—A hierarchical allostatic regulation model of medial prefrontal cortex function for social valuation. *Frontiers in Neuroscience*, 14, 281.
- Lawrence, K. E., Hernandez, L. M., Bowman, H. C., Padgaonkar, N. T., Fuster, E., Jack, A., Aylward, E., Gaab, N., van Horn, J. D., & Bernier, R. A. (2020). Sex differences in functional connectivity of the salience, default mode, and central executive networks in youth with ASD. *Cerebral Cortex*, 30, 5107–5120.
- Lefort-Besnard, J., Vogeley, K., Schilbach, L., Varoquaux, G., Thirion, B., Dumas, G., & Bzdok, D. (2020). Patterns of autism symptoms: Hidden structure in the ADOS and ADI-R instruments. *Translational Psychiatry*, 10, 1–12.
- Li, M., & Liu, K. (2019). Causality-based attribute weighting via information flow and genetic algorithm for naive Bayes classifier. *IEEE Access*, 7, 150630–150641.
- Liang, X. S. (2008). Information flow within stochastic dynamical systems. *Physical Review E*, 78, 031113-1–031113-15.
- Liang, X. S. (2014). Unraveling the cause-effect relation between time series. *Physical Review E*, 90, 052150.
- Liang, X. S. (2016a). Exploring the big data using a rigorous and quantitative causality analysis. *Journal of Computer and Communications*, 4, 53–59.
- Liang, X. S. (2016b). Information flow and causality as rigorous notions ab initio. *Physical Review E*, 94, 052201.
- Liang, X. S. (2021). Normalized multivariate time series causality analysis and causal graph reconstruction. *Entropy*, 23, 679.
- Liang, X. S., & Kleeman, R. (2005). Information transfer between dynamical system components. *Physical Review Letters*, 95, 244101.
- Liang, X. S., Xu, F., Rong, Y., Zhang, R., Tang, X., & Zhang, F. (2021). El Niño Modoki can be mostly predicted more than 10 years ahead of time. *Scientific Reports*, 11, 1–14.
- Liu, F., Guo, W., Fouche, J.-P., Wang, Y., Wang, W., Ding, J., Zeng, L., Qiu, C., Gong, Q., & Zhang, W. (2015). Multivariate classification of social anxiety disorder using whole brain functional connectivity. *Brain Structure and Function*, 220, 101–115.
- Lizier, J. T., & Prokopenko, M. (2010). Differentiating information transfer and causal effect. *The European Physical Journal B*, 73, 605–615.
- Lombardo, M. V., Eyler, L., Moore, A., Datko, M., Barnes, C. C., Cha, D., Courchesne, E., & Pierce, K. (2019). Default mode-visual network hypoconnectivity in an autism subtype with pronounced social visual engagement difficulties. *eLife*, 8, e47427.
- Lord, C., Risi, S., Lambrecht, L., Cook, E. H., Leventhal, B. L., DiLavore, P. C., Pickles, A., & Rutter, M. (2000). The autism diagnostic observation schedule—Generic: A standard measure of social and communication deficits associated with the spectrum of autism. *Journal of Autism and Developmental Disorders*, 30, 205–223.
- Lord, C., Rutter, M., & Le Couteur, A. (1994). Autism diagnostic interview—revised: A revised version of a diagnostic interview for caregivers of individuals with possible pervasive developmental disorders. *Journal of Autism and Developmental Disorders*, 24, 659–685.
- Lynch, C. J., Uddin, L. Q., Supekar, K., Khouzam, A., Phillips, J., & Menon, V. (2013). Default mode network in childhood autism: Posteromedial cortex heterogeneity and relationship with social deficits. *Biological Psychiatry*, 74, 212–219.
- Maggi, S., & Humphries, M. D. (2022). Activity subspaces in medial prefrontal cortex distinguish states of the world. *Journal of Neuroscience*, 42, 4131–4146.
- Mars, R. B., Neubert, F.-X., Noonan, M. P., Sallet, J., Toni, I., & Rushworth, M. F. (2012). On the relationship between the “default mode network” and the “social brain”. *Frontiers in Human Neuroscience*, 6, 189.
- Martin, A. K., Dzafic, I., Ramdave, S., & Meinzer, M. (2017). Causal evidence for task-specific involvement of the dorsomedial prefrontal cortex in human social cognition. *Social Cognitive and Affective Neuroscience*, 12, 1209–1218.
- McCracken, J. M. (2016). Exploratory causal analysis with time series data. *Synthesis Lectures on Data Mining and Knowledge Discovery*, 8, 1–147.
- Monk, C. S., Peltier, S. J., Wiggins, J. L., Weng, S.-J., Carrasco, M., Risi, S., & Lord, C. (2009). Abnormalities of intrinsic functional connectivity in autism spectrum disorders. *NeuroImage*, 47, 764–772.
- Murphy, K., Birn, R. M., Handwerker, D. A., Jones, T. B., & Bandettini, P. A. (2009). The impact of global signal regression on resting state correlations: Are anti-correlated networks introduced? *NeuroImage*, 44, 893–905.
- Murphy, K., & Fox, M. D. (2017). Towards a consensus regarding global signal regression for resting state functional connectivity MRI. *NeuroImage*, 154, 169–173.
- Nielsen, J. A., Zielinski, B. A., Fletcher, P. T., Alexander, A. L., Lange, N., Bigler, E. D., Lainhart, J. E., & Anderson, J. S. (2014). Abnormal lateralization of functional connectivity between language and default mode regions in autism. *Molecular Autism*, 5, 1–11.
- Nobusako, S., Nishi, Y., Nishi, Y., Shuto, T., Asano, D., Osumi, M., & Morioka, S. (2017). Transcranial direct current stimulation of the temporoparietal junction and inferior frontal cortex improves imitation-inhibition and perspective-taking with no effect on the autism-spectrum quotient score. *Frontiers in Behavioral Neuroscience*, 11, 84.

- Padmanabhan, A., Lynch, C. J., Schaer, M., & Menon, V. (2017). The default mode network in autism. *Biological Psychiatry*, 2, 476–486.
- Paine, T. A., Swedlow, N., & Swetschinski, L. (2017). Decreasing GABA function within the medial prefrontal cortex or basolateral amygdala decreases sociability. *Behavioural Brain Research*, 317, 542–552.
- Power, J. D., Barnes, K. A., Snyder, A. Z., Schlaggar, B. L., & Petersen, S. E. (2012). Spurious but systematic correlations in functional connectivity MRI networks arise from subject motion. *NeuroImage*, 59, 2142–2154.
- Raichle, M. E., MacLeod, A. M., Snyder, A. Z., Powers, W. J., Gusnard, D. A., & Shulman, G. L. (2001). A default mode of brain function. *Proceedings of the National Academy of Sciences*, 98, 676–682.
- Rolls, E. T., Zhou, Y., Cheng, W., Gilson, M., Deco, G., & Feng, J. (2020). Effective connectivity in autism. *Autism Research*, 13, 32–44.
- Rubinov, M., & Sporns, O. (2010). Complex network measures of brain connectivity: Uses and interpretations. *NeuroImage*, 52, 1059–1069.
- Rudie, J. D., Brown, J., Beck-Pancer, D., Hernandez, L., Dennis, E., Thompson, P., Bookheimer, S., & Dapretto, M. (2013). Altered functional and structural brain network organization in autism. *NeuroImage: Clinical*, 2, 79–94.
- Salehi, F., Jaloli, M., Coben, R., & Nasrabadi, A. M. (2022). Estimating brain effective connectivity from EEG signals of patients with autism disorder and healthy individuals by reducing volume conduction effect. *Cognitive Neurodynamics*, 16, 519–529.
- Salehinejad, M. A., Paknia, N., Hosseinpour, A. H., Yavari, F., Vicario, C. M., Nitsche, M. A., & Nejati, V. (2021). Contribution of the right temporoparietal junction and ventromedial prefrontal cortex to theory of mind in autism: A randomized, sham-controlled tDCS study. *Autism Research*, 14, 1572–1584.
- Santana, C. P., de Carvalho, E. A., Rodrigues, I. D., Bastos, G. S., de Souza, A. D., & de Brito, L. L. (2022). rs-fMRI and machine learning for ASD diagnosis: A systematic review and meta-analysis. *Scientific Reports*, 12, 1–20.
- Saxe, R., & Kanwisher, N. (2003). People thinking about thinking people: The role of the temporo-parietal junction in “theory of mind”. *NeuroImage*, 19, 1835–1842.
- Schilbach, L., Eickhoff, S. B., Rotarska-Jagiela, A., Fink, G. R., & Vogeley, K. (2008). Minds at rest? Social cognition as the default mode of cognizing and its putative relationship to the “default system” of the brain. *Consciousness and Cognition*, 17, 457–467.
- Schreiber, T. (2000). Measuring information transfer. *Physical Review Letters*, 85, 461–464.
- Schulte-Rüther, M., Greimel, E., Markowitsch, H. J., Kamp-Becker, I., Remschmidt, H., Fink, G. R., & Piefke, M. (2011). Dysfunctions in brain networks supporting empathy: An fMRI study in adults with autism spectrum disorders. *Social Neuroscience*, 6, 1–21.
- Schultz, D. H., & Cole, M. W. (2016). Higher intelligence is associated with less task-related brain network reconfiguration. *Journal of Neuroscience*, 36, 8551–8561.
- Seth, A. K. (2010). A MATLAB toolbox for Granger causal connectivity analysis. *Journal of Neuroscience Methods*, 186, 262–273.
- Smallwood, J., Bernhardt, B. C., Leech, R., Bzdok, D., Jefferies, E., & Margulies, D. S. (2021). The default mode network in cognition: A topographical perspective. *Nature Reviews Neuroscience*, 22, 503–513.
- Sridharan, D., Levitin, D. J., & Menon, V. (2008). A critical role for the right fronto-insular cortex in switching between central-executive and default-mode networks. *Proceedings of the National Academy of Sciences*, 105, 12569–12574.
- Storey, J. D. (2002). A direct approach to false discovery rates. *Journal of the Royal Statistical Society: Series B (Statistical Methodology)*, 64, 479–498.
- Talebi, N., Nasrabadi, A. M., Mohammad-Rezazadeh, I., & Coben, R. (2019). NCREANN: Nonlinear causal relationship estimation by artificial neural network; applied for autism connectivity study. *IEEE Transactions on Medical Imaging*, 38, 2883–2890.
- Trakoshis, S., Rocchi, F., Canella, C., You, W., Chakrabarti, B., Ruigrok, A. N., Bullmore, E. T., Suckling, J., Markicevic, M., & Zerbib, V. (2020). Intrinsic excitation-inhibition imbalance affects medial prefrontal cortex differently in autistic men versus women. *eLife*, 9, e55684.
- Venkatesh, P., & Grover, P. (2015). *Is the direction of greater Granger causal influence the same as the direction of information flow?* (pp. 672–679). IEEE.
- Wang, X., Wang, R., Li, F., Lin, Q., Zhao, X., & Hu, Z. (2020). Large-scale granger causal brain network based on resting-state fMRI data. *Neuroscience*, 425, 169–180.
- Yan, C., & Zang, Y. (2010). DPARSF: A MATLAB toolbox for “pipeline” data analysis of resting-state fMRI. *Frontiers in Systems Neuroscience*, 4, 13.
- Yerys, B. E., Gordon, E. M., Abrams, D. N., Satterthwaite, T. D., Weinblatt, R., Jankowski, K. F., Strang, J., Kenworthy, L., Gaillard, W. D., & Vaidya, C. J. (2015). Default mode network segregation and social deficits in autism spectrum disorder: Evidence from non-medicated children. *NeuroImage: Clinical*, 9, 223–232.
- Yi, B., & Bose, S. (2022). Quantum Liang information flow as causation quantifier. *Physical Review Letters*, 129, 020501.
- Zhang, T., Cong, J., Li, F., Yao, D., & Xu, P. (2021). Causal network connectivity patterns in autism spectrum disorder based on the Liang-Kleeman information flow theory. *International Journal of Psychophysiology*, 168, S219–S220.
- Zhang, T., Wang, F., Li, M., Li, F., Tan, Y., Zhang, Y., Yang, H., Biswal, B., Yao, D., & Xu, P. (2019). Reconfiguration patterns of large-scale brain networks in motor imagery. *Brain Structure and Function*, 224, 553–566.
- Zhao, H., Lv, R., Cai, X., & Zhang, G. (2021). Changes of entropy connectivity of the default mode and central executive networks in ASD.

SUPPORTING INFORMATION

Additional supporting information can be found online in the Supporting Information section at the end of this article.

How to cite this article: Cong, J., Zhuang, W., Liu, Y., Yin, S., Jia, H., Yi, C., Chen, K., Xue, K., Li, F., Yao, D., Xu, P., & Zhang, T. (2023). Altered default mode network causal connectivity patterns in autism spectrum disorder revealed by Liang information flow analysis. *Human Brain Mapping*, 44(6), 2279–2293. <https://doi.org/10.1002/hbm.26209>